DMAP Immobilized on Porous Silica Particles and Monoliths for the Esterification of Phenylethanol in Continuous Flow

Julia S. Schulze,[a] Raoul D. Brand,[a] Joachim G. C. Hering,[a] Luise M. Riegger,[a] Peter R. Schreiner,[b, c] and Bernd M. Smarsly*[a, c]

We report the immobilization of 4-dimethylaminopyridine (DMAP), a versatile organocatalyst for sterically demanding esterifications, on mesoporous silica particles and macro-mesoporous silica monoliths, both possessing optimized properties for continuous flow synthesis. An alkyne-functionalized DMAP derivative was immobilized via click chemistry; the materials were characterized by physisorption analysis, diffuse reflectance infrared Fourier transform spectroscopy (DRIFT) and elemental analysis. While silica particles were functionalized in batch and packed into a packed-bed reactor, monoliths were cladded with a polyether ether ketone (PEEK) tube after sol-gel synthesis and functionalized in a circulating flow process. Samples with three different catalyst loadings were prepared, in order to study the impact of the catalyst amount on the mesopore space as well as the catalytic performance. In continuous flow experiments, complete conversion of 1-phenylethanol to phenylethylacetate was achieved with both materials and short contact times. Monoliths exhibited far lower pressures than packed bed reactors (7 bar at a flow rate of $1 \, \text{mL} \, \text{min}^{-1}$) and reached turnover rates up to $9.3 \times 10^{-2} \, \text{s}^{-1}$, which is almost twice as high as a comparable batch experiment. The absence of diffusion limitations in monoliths made investigations on reaction kinetics with microkinetics-dominated experiments possible. This study demonstrates that all properties needed for a successful transfer of immobilized organocatalysts to sophisticated flow syntheses with complex organocatalysts can be met with functionalized meso-macroporous monoliths.

Introduction

4-Dimethylaminopyridine (DMAP) is a nucleophilic catalyst best known for its use in the Steglich esterification (scheme 1).[1,2] It is of great value for chemical synthesis because it catalyzes a large variety of group-transfer reactions, ranging from acylations of alcohols and amines, silylations and ester rearrangements to polymerizations, and named reactions like the Baylis-Hillman reaction.[3–7] With chiral DMAP derivatives, even enantioselective reactions are possible.[8,9] In addition to its versatile applications, DMAP is able to handle sterically hindered substrates like tertiary alcohols. This versatility makes it an indispensable catalyst for research laboratories, but it is also used for large-scale applications.

In industry, DMAP is mainly used for esterification in fine chemical production like flavor and fragrance industries, or pharmaceuticals. Especially for elaborate pharmaceutical drugs, the ability to convert large and sterically hindered substrates is of great value. For example, DMAP is used for catalyzing esterifications of important steps during multistep syntheses of drugs like cholesterol-lowering statins,[10] taxanes for chemotherapy,[11] or vitamin E derivatives.[12]

Since DMAP is toxic, meticulous purification is necessary to avoid catalyst traces in the product. In general, immobilizing organocatalysts on solid supports is of great potential and value for easy separation and reusability, and it simplifies work-up. Catalyst recycling and fewer purification steps are also useful from a green chemistry point of view, and - especially for expensive organocatalysts that require high catalyst loadings - easy recycling and reuse can bring economic advantages.

Polymers, silica, magnetic nanoparticles and several more have been used for immobilization of catalytic motives.[13–15] Silica is a suitable solid support for many applications because of its thermal and mechanical stability, low cost, and chemical inertness to common organic reaction conditions (with exception of very high pH values). Its main advantage is the flexibility in the controlled variation of material properties: pore size and shape, surface area, and morphology can be tailored to fit the needs of different applications. Because of that, many different silica materials have been used as solid support for organo-
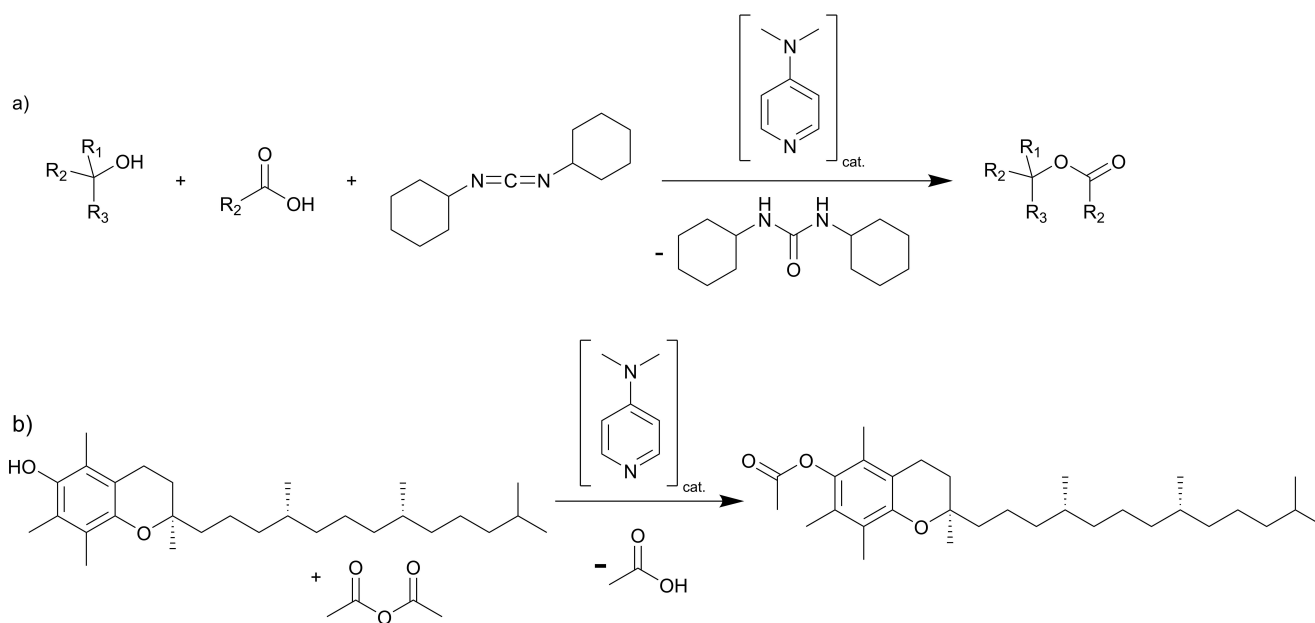
[a] J. S. Schulze, R. D. Brand, J. G. C. Hering, L. M. Riegger, B. M. Smarsly
     Institute of Physical Chemistry
     Justus Liebig University Giessen
     Heinrich-Buff-Ring 17
     D-35392 Giessen (Germany)
     E-mail: Bernd.Smarsly@phys.Chemie.uni-giessen.de
[b] P. R. Schreiner
     Institute of Organic Chemistry
     Justus Liebig University Giessen
     Heinrich-Buff-Ring 17
     D-35392 Giessen (Germany)
[c] P. R. Schreiner, B. M. Smarsly
     Center for Materials Research
     Heinrich-Buff-Ring 16
     D-35392 Giessen (Germany)

ChemCatChem

Research Article
doi.org/10.1002/cctc.202101845

Chemistry Europe
European Chemical
Societies Publishing

Scheme 1. Steglich esterification of tertiary alcohols catalyzed by DMAP (a) and example for esterification of α-tocopherol to α-tocopheryl acetate, allowing for longer shelf life (b).

catalysts, ranging from unordered silica gel to highly ordered SBA-15, and from particles to monoliths.[16–20]

The transfer of these materials to continuous flow reactors brings several additional advantages. Continuous processing, quick and precise heat control, short reaction times, and the possibility to carry out multi-step reactions without isolating intermediate products make continuous flow setups convenient; the large surface-to-volume ratio and easy scalability by numbering-up or scaling-out can lead to greater productivity.[21–23]

In batch, the morphology does not play a big role except for surface area and accessibility of pores, but in continuous flow additional requirements come into play. The pores of the material have to be easily accessible for bulky substrate molecules to produce small residence time distributions, and quick flow-through of reaction solution without creating a large pressure build-up is needed. Fortunately, there is no need to reinvent the wheel as existing materials can be used and adapted for catalysis. Silica materials for high-pressure liquid chromatography (HPLC) are already optimized for flow applications and can be modified to work as carrier materials for organocatalysts.

We focused on two different materials in this study. The first silica material are commercially available mesoporous silica particles optimized for HPLC. Because of their uniform shape and size, the particles can be packed into a dense and homogeneous way, which ensures good properties for operation in continuous flow. The second silica material are meso-macroporous monoliths synthesized after a modified "Nakanishi process".[24–26] This synthesis can be performed with good reproducibility, and thus these materials are commercialized for HPLC separation.[27–32] With their bimodal porosity comprising

macroporous flow-through space and a large surface area due to their mesoporosity, these SiO$_2$ monoliths are also promising solid supports for heterogeneous catalysis in continuous flow.[29,33,34] They combine high hydraulic permeability with low diffusion mass transfer resistance in the mesoporous skeleton. To use the monoliths in continuous flow experiments, they must be cladded and threaded to connect them to the system in a way that provides pressure stability, chemical inertness and durability. We used a process adapted from Chamieh et al. in which a PEEK tube is used as cladding.[35,36] By further optimizing this technique, we achieved control over all steps, encompassing sol-gel synthesis of the monoliths, functionalization, and finally generation of cladded, functionalized monoliths. Since we can control and analyze the properties of the reactor material from cradle to grave, we were thus able to modify the reactors along our needs with respect to the porosity and catalyst loading.

Several research groups have reported the immobilization of DMAP on solid supports. Besides various studies with polymers as solid supports,[37–39] porous silica has been used as carrier material for DMAP in form of undefined gels, in mesoporous morphologies like SBA-15 and MCM, or in core-shell-structured nanoparticles with magnetic cores and silica surface.[4,40–42] However, previous studies on heterogeneous DMAP catalysis in flow mainly use polymer materials,[43,44] but DMAP immobilization has not been done yet on silica materials optimized for flow conditions. Building on the promising previous works on DMAP immobilized on silica, substantial improvement can be expected by using the aforementioned particle-based on monolithic columns. Various problems can arise from functionalization of materials for flow applications: In case of packed-bed reactors, it is of great importance not to

ChemCatChem

Research Article
doi.org/10.1002/cctc.202101845

Chemistry Europe
European Chemical
Societies Publishing

damage the morphology of the particles. If their spherical shape is altered during functionalization, e.g., due to excessive stirring, the particles cannot be packed into the column properly and will possibly produce very high pressures in flow. Monoliths cannot be functionalized prior to cladding, because the temperature during the cladding process would degrade organic groups. Therefore, all functionalization steps have to be done in continuous flow. On the one hand, such processing is advantageous: The material properties that allow efficient transport during catalysis also provide good accessibility of the surface for functionalization reactions. On the other hand, additional parameters like the flow rate of the reagent solution have to be considered, or - in case of solubility of reactants - play a greater role in functionalization. The characterization of monoliths functionalized in a flow setup has to be performed meticulously, because the material cannot be handled as a homogeneous sample. Grafting gradients from functionalization in flow might be present and have to be accounted for with separate analysis of distinct monolith parts.

Most publications investigate the catalytic performance of one concentration of catalyst in the material. More catalyst on the surface might be beneficial for performance, but a too crowded surface might clog pores or sterically hinder substrate molecules from approaching the catalyst motives. To test what influence different catalyst loadings have, we prepared three materials with different catalyst loadings. Discussion between productivities of different material morphologies and comparison with batch experiments is important, but also challenging because of vastly different material properties and reaction setups. To tackle this issue, we used the easy tuneability of monolith meso- and macroporosity to match and to compare with the properties of the commercially available silica particles. Therefore, we were able to observe the effect of the additional macroporosity in the monoliths on performance in catalysis. To explore if our materials can compete with conventional batch catalysis, we conducted a heterogeneous batch experiment with our materials and compared the resulting turnover frequencies.[45]

Due to the fast establishment of steady states in continuous flow, sharp residence time distribution and absence of transport limitations in monolithic reactors, it is also possible to investigate kinetic parameters with experiments that are within the microkinetic range. Haas et al. used amine-functionalized monoliths of comparable properties for kinetic studies of the Knoevenagel condensation and found that activation energies in these reactors resemble homogeneous reactions.[46–48] To our knowledge, this has not been done yet with an immobilized DMAP derivative. The investigation of kinetic parameters is however inevitable to fully understand the reaction inside the reactor and optimize it for better yields.

For our tests, we used the conversion of 1-phenylethanol to phenylethylacetate, a reaction commonly used in literature to test performance of immobilized DMAP species. Since the wide substrate scope of DMAP has been well researched, we are confident that the positive results of this study will pave the way for these materials to be used with different and possibly more complex substrates like the pharmaceutical drugs men-

tioned in the beginning. In this work, we aim to bridge the gap between complex organocatalysts and sophisticated silica materials to build reactors for continuous flow organocatalysis. We demonstrate the potential of such reactors with a DMAP derivative immobilized on two silica materials designed for HPLC applications, addressing functionalization, characterization, catalytic and kinetic properties of the functionalized reactors.

Results and Discussion

Characterization of carrier material

Two different materials were used for immobilization of the DMAP organocatalyst. The first material, LiChrospher Si 100 5 μm, is an HPLC material optimized for flow applications consisting of fully mesoporous silica particles. It was chosen because of its good performance and commercial applications in HPLC, where the uniform spherical shape of the particles leads to homogeneous and optimized packing, which results in advantageous flow properties, e.g., in terms of the transcolumn homogeneity. The second material is a monolithic silica material with hierarchical meso-macroporosity that leads to high hydraulic permeability of 1.0×10^{-13} m^2 due to the special macroporosity and a large surface area for functionalization due to the pronounced mesoporosity (see Table 1 for an overview). The total porosity is calculated from meso- and macroporosity for monoliths, and from mesoporosity and interparticle voids for particles. For monoliths, the total porosity (meso- and macroporosity) ε_{total} is 86%, while the porosity of the packed particles inside the columns is about 80%, which is substantially lower than for the monolithic silica columns. Hence, the hydraulic permeability of such packed-bed reactors can be calculated to 6×10^{-15} m^2 being thus significantly lower compared to the meso-macroporous SiO$_2$ monoliths. In conclusion, both types of columns are feasible for HPLC separation, and with these materials used as a solid support, low and reproducible pressure build-up can be expected in continuous flow catalysis. The monolithic silica additionally features advection-dominated transport of liquids through the macroporous space, which in turn might translate into high catalytic performance if used as a solid support for catalysis in flow.

Table 1. Properties of mesoporous silica particles and macro-mesoporous silica monoliths. ε_{macro} referenced to total column volume, ε_{meso} to skeleton volume.

	monoliths	particles
mesoporosity		
d_{meso} [nm]	13	11
V_{meso} [mL g^{-1}]	0.9	1.2
ε_{meso}	0.66	0.72
macroporosity		
d_{macro} [μm]	2.5	–
V_{macro} [mL g^{-1}]	2.3	–
ε_{macro}	0.63	–

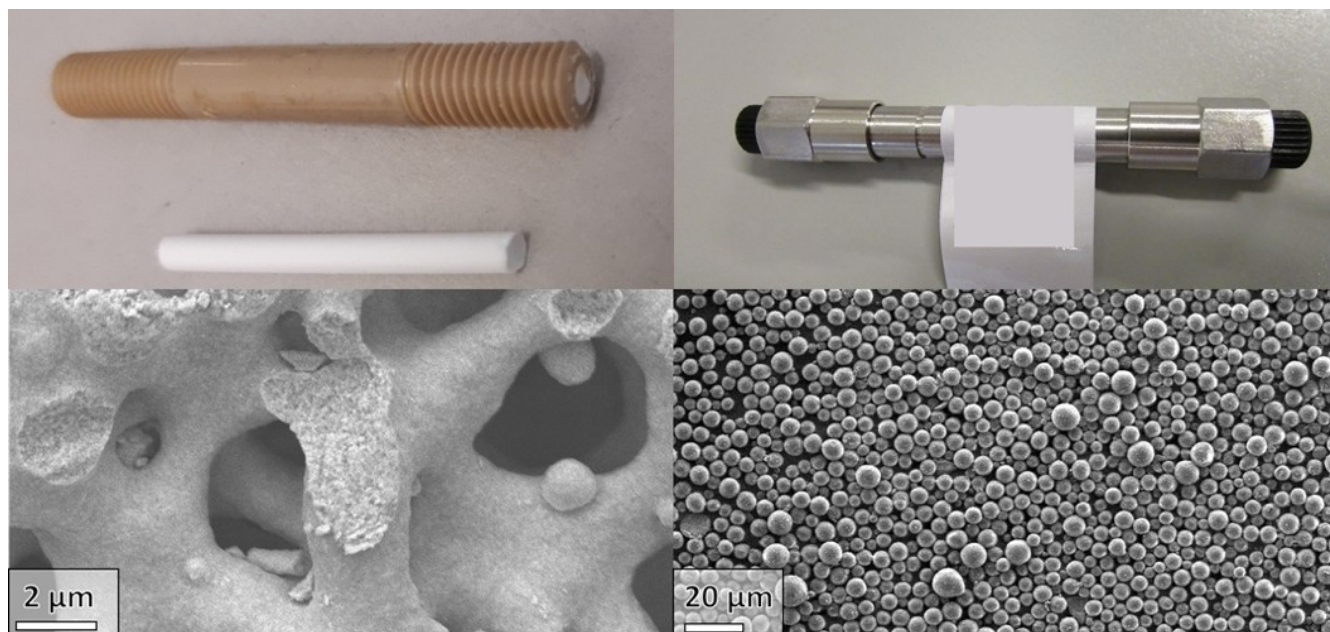**Figure 1.** Photographs (top) and SEM images (bottom) of silica monoliths (left) and silica particles (right). Inner dimensions are Ø 3 mm×5 cm for monolithic reactors and Ø 4 mm×5 cm for packed-bed columns (particle size 5 μm).

Figure 1 shows SEM images of the different materials and pore sizes.

Preparation and characterization of catalyst material

Prior to functionalization, the monoliths were cladded in PEEK. PEEK was fit tightly onto the rods by inserting it into a PTFE shrinking tube and heating it just below the melting point of PEEK. The softened PEEK envelope is pressed against the silica due to the shrinking tube and a tight connection between cladding and material is created.[35,36]

A copper-catalyzed cycloaddition was used for immobilization of a DMAP derivative on silica (Scheme 2). First, (3-azidopropyl)trimethoxysilane (Az-PTMS) was grafted onto the material (Scheme 2 a). Varying the amount of Az-PTMS resulted in materials with different azide loadings. Toluene was chosen as solvent for the first functionalization step, because it enables a homogeneous functionalization. Since it is an aprotic solvent, a defined amount of water or triethylamine was needed to promote condensation. Silica particles were functionalized in a batch reaction, while monoliths were functionalized with a circular flow setup where the silane solution was passed through the monolith several times. The success of the grafting step was quantified by elemental analysis. For analysis, the reactor was sawed into pieces, but small contaminations of the SiO_2 material with PEEK due to sawing can lead to unreliable carbon content values. To evade this effect, the azide loading was calculated based on the nitrogen content and additionally confirmed through the intensity of the azide band with DRIFT spectroscopy, as well as with the decrease in pore volume determined by nitrogen physisorption experiments (Figures 2
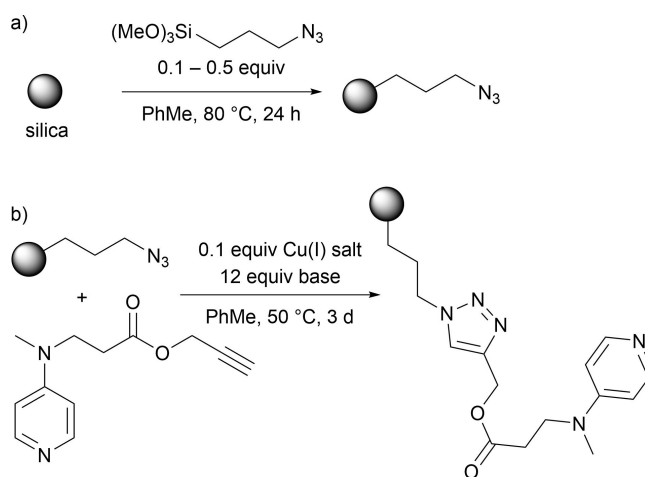
Scheme 2. Synthesis route for immobilization of DMAP on mesoporous silica particles. Monoliths were functionalized in a similar way in continuous flow.

and 3). All physisorption data were normalized to silica mass for a meaningful depiction of the effect of grafting on the potential filling or blocking of mesoporosity. The physisorption analysis shows a type IVa isotherm with a pronounced hysteresis, the shape of which is in accordance with previous reports on such monolithic silica.[49] We observed that the mesopore volume significantly decreased upon functionalization already with the azide-containing silane, for both the monoliths and the SiO_2 particles (table 2). Since the adsorbed volumes were normalized to the mass of bare SiO_2, the decrease in specific pore volume is indeed due to the partial occupation of mesopore space by the organic moieties, and not blurred by the increased mass due to the functionalization. Yet, the shape of the isotherms was
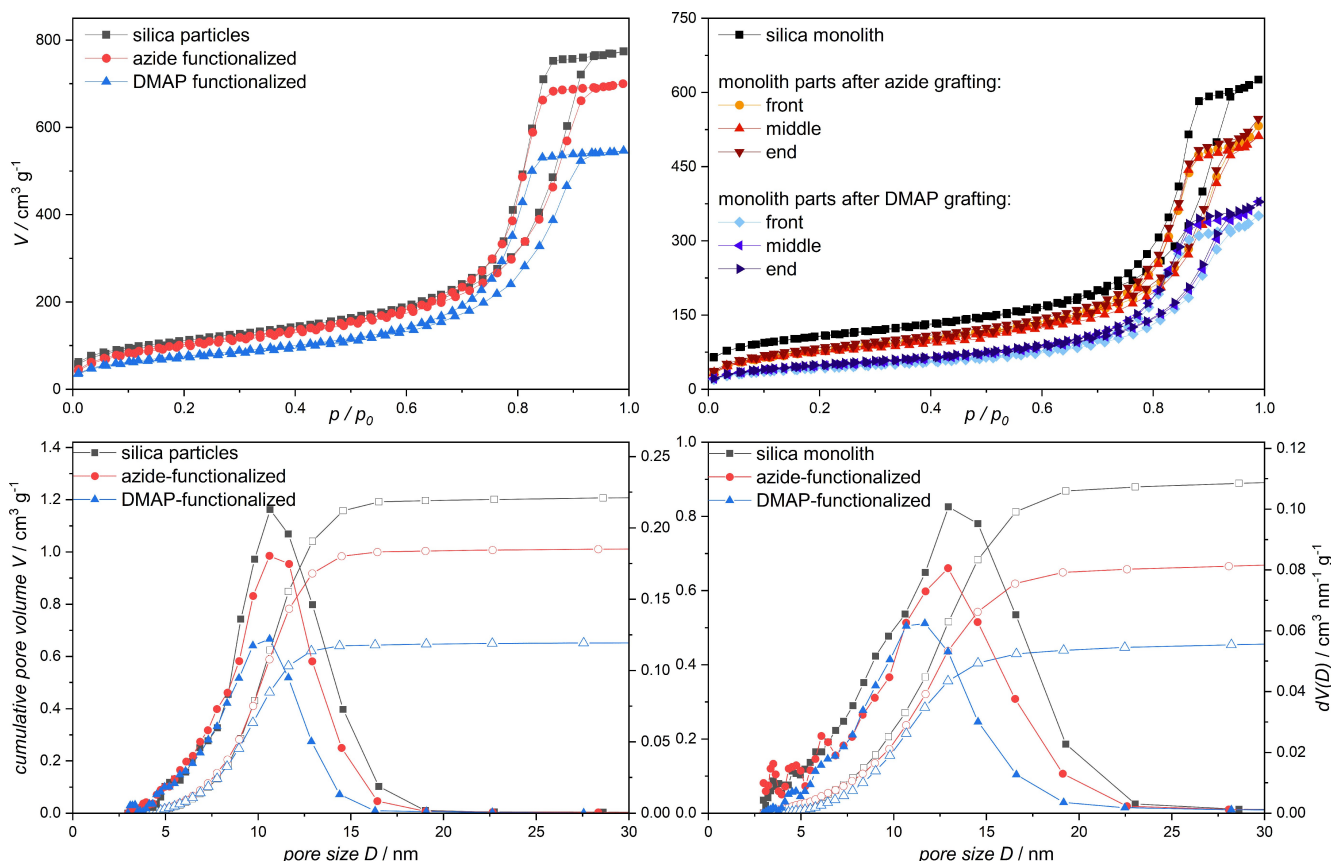
ChemCatChem

Research Article
doi.org/10.1002/cctc.202101845

Chemistry
Europe
European Chemical
Societies Publishing

Figure 2. Top row: Nitrogen physisorption isotherms of monolithic silica and silica particles as synthesized, after azide grafting, and after DMAP grafting (each with the highest loading of 0.7 and 0.8 mmol g^{-1} respectively). Note that the pore volume of the functionalized samples was normalized to the mass of bare SiO$_2$, not to the mass of the functionalized SiO$_2$. Such normalization is more suitable to detect a decrease in mesopore volume and hence a surface functionalization, compared to the non-functionalized SiO$_2$ materials. Bottom row: Pore size distributions of untreated and functionalized silica monoliths (left) and particles (right).
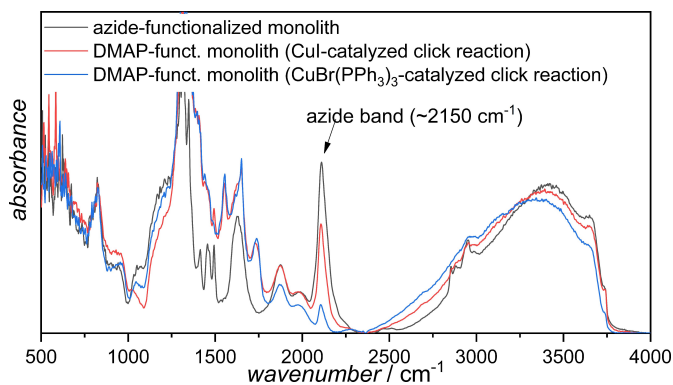

Figure 3. DRIFT spectra of an azide functionalized monolith (0.5 mmol g^{-1}), and DMAP monolith after click-reaction with CuI or CuBr(PPh$_3$)$_3$. The intensity of the azide band gives an estimation of the amount of remaining azide groups after the click-reaction.

Table 2. Physisorption data of silica monoliths and particles before and after the two grafting steps (0.7 mmol g^{-1}).

	d_{meso} [nm]	V_{meso} [mL g^{-1}]	BET area [m^2 g^{-1}]
monoliths			
unfunctionalized	13	0.9	340
azide	12	0.7	240
DMAP	11	0.5	140
particles			
unfunctionalized	11	1.2	380
azide	11	1.0	330
DMAP	10	0.7	190

almost identical after incorporation of the DMAP-containing organic moiety, speaking for a surface coverage without clogging of the mesopore space. The incorporation of the azide group within the mesopores is further demonstrated by the decline in the average pore size (mode value) and the overall shift of the mesopore size distribution towards smaller dimension.

The DMAP derivative was immobilized via a copper-catalyzed alkyne azide cycloaddition, in which the alkyne group of the DMAP derivative reacts with the immobilized azide. This click chemistry method is often used for immobilization of molecules on surfaces because of its mild reaction conditions and lack of by-products.[50,51] A copper(I) salt is necessary to catalyze the reaction. For silica particles, copper iodide gave good conversion of azide groups, while monoliths were functionalized with better conversion using [CuBr(PPh$_3$)$_3$],

ChemCatChem

Research Article
doi.org/10.1002/cctc.202101845

**Chemistry
Europe**
European Chemical
Societies Publishing

presumably because of the greater solubility of [CuBr(PPh$_3$)$_3$] in toluene. While the solubility of the copper(I) salt is irrelevant in the batch functionalization of particles, it is crucial for the functionalization of monoliths in continuous flow. DRIFT measurements of the samples containing the azide moiety and finally the DMAP function reveal a significant decrease in the azide signal, the decline being more pronounced in case of using [CuBr(PPh$_3$)$_3$] (Figure 3). The monoliths were cut into three pieces that were analyzed separately to ensure that indeed uniform functionalization was achieved over the whole length of the monolith. The successful immobilization of the organo-catalyst is verified by elemental analysis, the vanishing of the azide band in DRIFT measurements, and by a further decrease in adsorbed pore volume.

Applying a rough calculation assuming an even distribution of catalyst on the surface, a cylindrical/spherical form and a sharp pore size distribution centred at 12 nm, the decrease in pore volume from 0.9 to 0.45 cm^3 g^{-1} accounts for an organic layer of approximately 1.2 nm inside the mesoporous space. The actual pore size distribution derived from physisorption shows a preferred functionalization of mesopores > 10 nm for both materials (Figure 2). One exemplary sample was examined with X-ray photoelectron spectroscopy to check for the presence of copper residues, and indeed no copper was found in the sample after washing (see ESI).

Particles with measured catalyst loadings of 0.3, 0.5, and 0.8 mmol g^{-1} and monoliths with a loading of 0.2, 0.5, and 0.7 mmol g^{-1} were synthesized to test the influence of different catalyst loadings on reaction performance. The particles were

packed into a stainless steel column (length 5 cm, diameter 0.4 cm).

Heterogeneous catalysis in continuous flow

We used the esterification of 1-phenylethanol with acetic acid anhydride as a test reaction to examine catalyst performance Figure 4). Toluene was chosen as the solvent after preliminary homogeneous tests with various solvents. Unfunctionalized monoliths showed no conversion at a flow rate of 0.05 mL min^{-1}. Continuous flow experiments revealed that full conversion of phenylethanol to phenylethyl acetate is possible with both reactor types using 0.3 M substrate in toluene with 1.5 eq. acetic anhydride and a slight excess of auxiliary base (1.5 eq. triethylamine, Figure 5). The reaction time is defined by the contact time of the reaction solution with the catalyst material, therefore the conversion increased with lower flow rates. For packed-bed columns, there is a clear trend: when looking at flow rates of 0.2 mL min^{-1} or higher, the material with the highest loading of 0.8 mmol g^{-1} DMAP led to the highest conversion, followed by the medium (0.6 mmol g^{-1}) loaded material. At low flow rates, this effect cannot be seen because all packed-bed reactors reach full conversion. While the observation that more catalyst equals greater conversion is not particularly surprising, this clear trend cannot be found in the monolithic reactors. Since it was not possible to prepare monoliths with higher catalyst amounts than 0.7 mmol g^{-1}, it is likely that the silica surface is fully covered with catalyst and some catalyst molecules cannot be reached by substrate
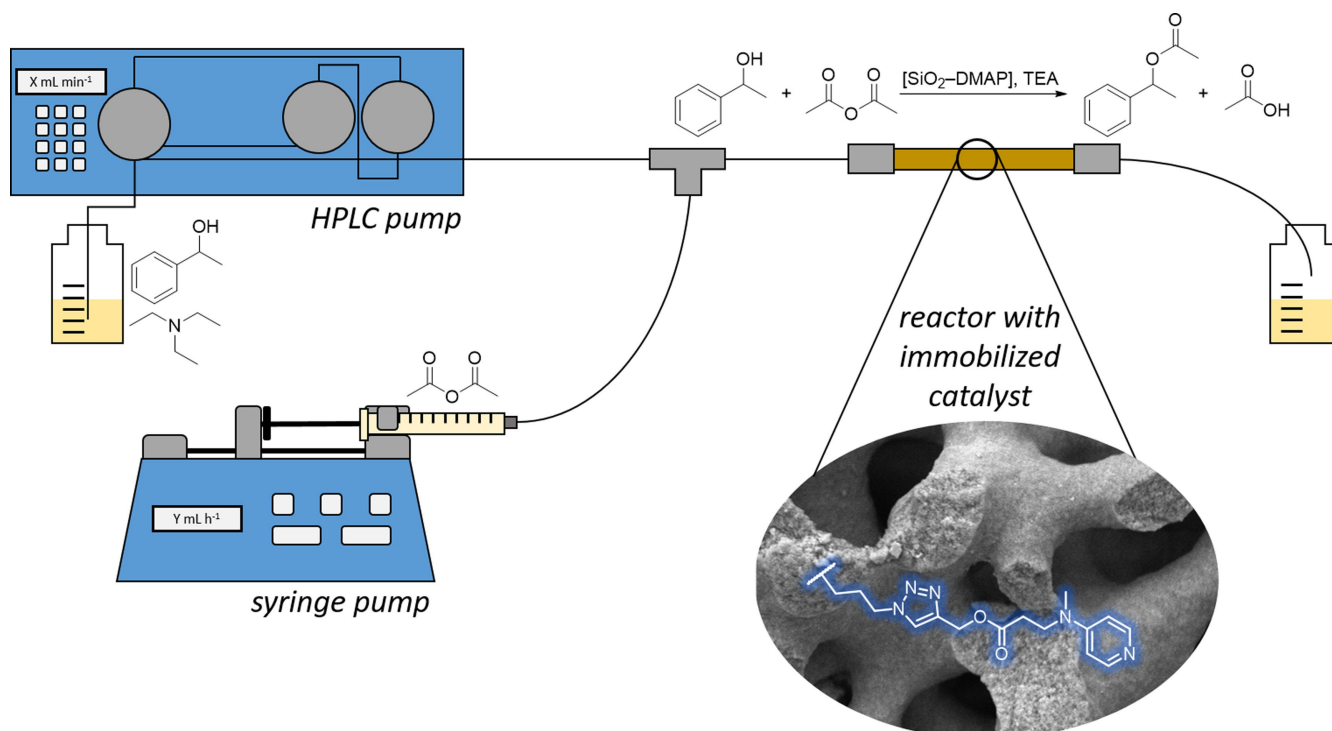

Figure 4. Reactor setup for continuous flow esterification (not to scale).
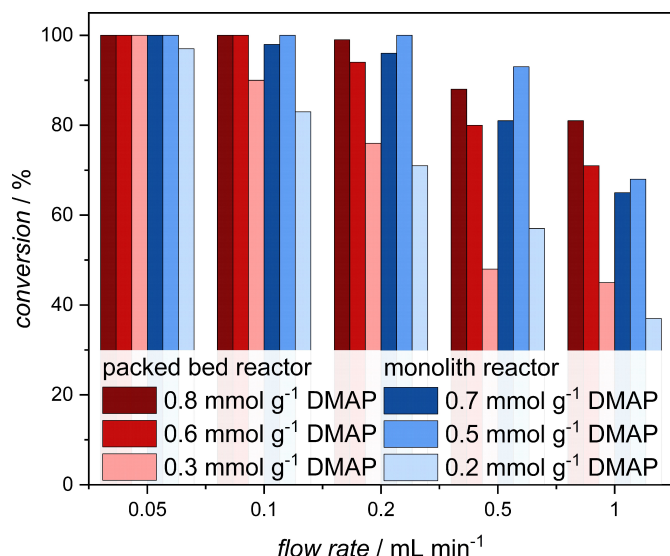
Figure 5. Conversion of 1-phenylethanol to 1-phenylethyl acetate using packed-bed (300 mg) and monolithic (100 mg) reactors of DMAP-functionalized silica with three different catalyst loadings (0.3 M substrate solution in toluene with 1.5 eq. acetic anhydride and triethylamine).

Figure 6. Comparison of turnover frequencies (TOFs) for monoliths (M) and packed-bed reactors (P) with different loadings (mmol g^{-1}).

molecules efficiently. The actual active loading can therefore be lower than the formal amount of catalyst in the reactor. The slightly higher BET surface area of the packed-bed silica particles might be a reason why this effect was not detected with packed-bed reactors.

Both reactors showed similar behavior in flow rate tests with minor differences in conversion. The overall efficiency of the materials was evaluated with turnover frequencies (TOF) calculated with Equation (1).

$$TOF = \frac{c_{product}F}{n_{cat}} \qquad (1)$$

$c_{product}$ = concentration of product, F = flow rate, n_{cat} = amount of catalyst

The TOF does not only account for conversion and time, but also includes the absolute amount of catalyst in the reactor. This is important for a meaningful comparison of packed-bed and monolithic reactors, because they differ in the material needed to build a reactor. A packed-bed reactor was filled with approx. 300 mg functionalized material, while a silica monolith only weighs 100 mg. This means that for similar conversions, three times the material is needed for the packed-bed reactors.

Figure 6 shows the TOF values of different materials. For both materials, increasing the flow rate leads to a higher TOF. Monolithic reactors, regardless of their DMAP loading, showed significantly higher TOF values than packed-bed reactors-here the difference in material amount that is needed for the same performance clearly comes into effect. The reason for this might be found in the porosity differences in the two materials. As shown before, both particles and monoliths are functionalized very homogeneously. During flow experiments, the accessibility of the functionalized pores decides if the immobilized catalyst
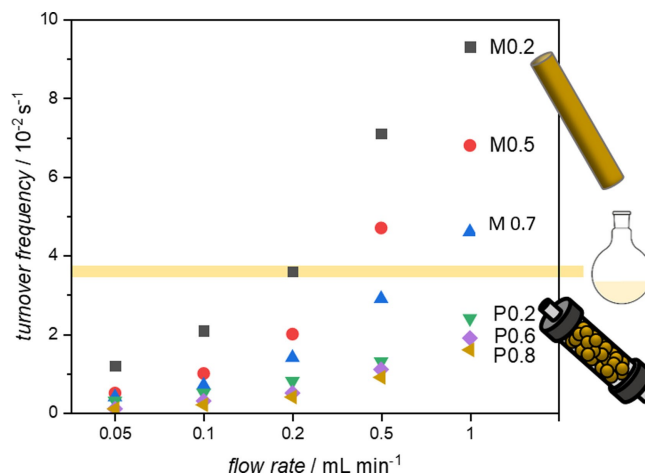
participates in the reaction. Since the skeleton thickness of the monoliths is smaller than the diameter of a particle, the inner pore network can be more easily accessed by substrate molecules, which means that the proportion of active catalyst sites is higher. The TOFs of the monolithic reactor were at a comparable level with TOF values of industrial catalyst applications, which typically range from 10^{-2} to 10^2 s^{-1}.[52] For flow rates above 0.5 mL min^{-1}, monolithic reactors also showed higher productivity than the reference batch experiment with powdered material (0.5 mmol g^{-1}, Table 3). The TOF for batch reactions was calculated using a reaction time with yields comparable to the highest flow rate of packed-bed and monolithic reactors. Reaction times $t_{reaction}$ for the continuous flow setups correspond to the residence time of the solution inside the reactor [Equation (2)].

$$t_{reaction} = \frac{(V_{macro} + V_{meso}) \cdot m_{reactor}}{F} \qquad (2)$$

Another remarkable difference can be found in back pressures required to pump the reaction mixture through the reactors. Figure 7 shows the superiority of monolithic bimodal pore structures over packed-bed reactors in terms of pressure build-up in the reactor. Low pressures are beneficial, because longer or multiple reactors and higher flow rates can be used without exceeding pressure limits of the equipment, leading to higher conversion with shorter retention times. For flow rates below 0.2 mL min^{-1}, the pressure drop over the monoliths was negligibly small. The pressure build-up increased moderately

Table 3. Comparison of turnover frequencies and reaction times for three reactor types (batch (5 % cat.), packed-bed, and monolith) with a material loaded with 0.5 mmol g^{-1} DMAP derivative.

	batch	packed-bed	monolith
TOF [10^{-2} s^{-1}]	3.7	1.9	6.8
$t_{reaction}$ [min]	30	0.3	0.3

ChemCatChem

Research Article
doi.org/10.1002/cctc.202101845

**Chemistry
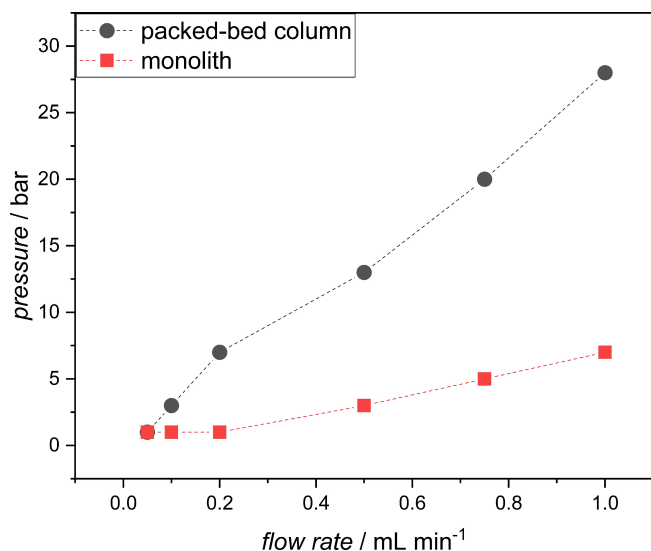Europe**
European Chemical
Societies Publishing

Figure 7. Comparison of pressure build-up for packed-bed and monolithic reactors with various flow rates.

for monoliths at higher flow rates, while a significant increase was observed for packed-bed columns.

During reaction, DMAP takes part in an acyl group transfer and is protonated and deprotonated constantly, therefore long-term stability of the material is a potential issue. We carried out a long-term test to determine the stability of the immobilized catalyst: During 20 h of continuous use with 0.2 mL min^{-1} substrate solution, we found no loss of conversion (see ESI). For long-time continuous reactions, either acetic acid anhydride or triethylamine needs to be added with a separate pump to avoid decomposition to acetic acid over time.

Reaction order and activation energy

Since Haas et al. showed that functionalized monoliths with a bimodal pore structure exhibit no transport limitations, it is possible to investigate kinetic properties of the catalyzed reaction with a series of flow rate, concentration and temperature experiments.[46] Mechanism and reaction order of esterifications with DMAP have been well studied by experimental and computational approaches.[53,54] To our knowledge, there are no reports of kinetic properties for DMAP as a heterogeneous catalyst in flow reactors. Since it is not self-evident that the reaction proceeds in the same way as in homogeneous batch experiments, our first step was to determine the reaction order. Therefore, initial reaction rates for various starting concentrations of phenylethanol (PE) and acetic acid (Ac$_2$O) were studied with a series of experiments with a 0.5 mmol g^{-1} DMAP functionalized monolith (Figure 8 a). Flow rates corresponding to reaction times between 2.4 and 40 s were investigated, but only reaction times <11 s were used for analysis to stay within the range of microkinetics. Equation (3) and (4) give the relation between reaction rate v and reaction orders a and b.

$$v = k \cdot c(PE)^a \cdot c(Ac_2O)^b \tag{3}$$

$v =$ reaction rate, $k =$ reaction rate coefficient, $a, b =$ reaction order of PE, Ac$_2$O

$$\ln v = \ln k + a \cdot \ln c(PE) + b \cdot \ln c(Ac_2O) = \ln k' + a \cdot \ln c(PE) \tag{4}$$

For both PE and Ac$_2$O a first-order behaviour was found, leading to an overall reaction order of two (Figure 8b and ESI), which is in agreement with the homogeneously catalysed reaction.

Since Haas et al. showed that this type of silica monoliths exhibit small Thiele moduli ($\sim 10^{-4}$), meaning that transport
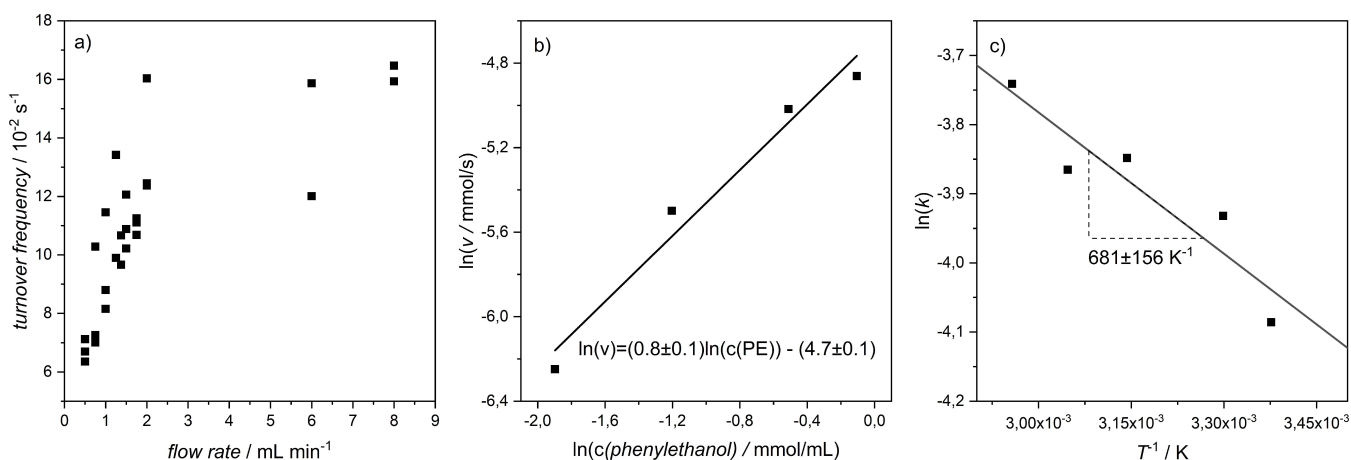

Figure 8. Turnover frequency of conversion from 0.3 M phenylethanol to phenylethyl acetate with a 0.5 mmol g^{-1} DMAP-loaded monolith at different flow rates (a), determination of reaction order by correlation between initial reaction rate v and starting concentration of substrate (b), and determination of activation energy via linearized Arrhenius plot (c).

limitations are absent, the activation energy of the reaction can be calculated by measuring the influence of temperature on the reaction rate coefficient k. In a plot of the linearized Arrhenius equation, the activation energy is revealed by the slope of the fit [Equation (5)].

$$\ln k = \ln A - \frac{E_a}{R} \cdot \frac{1}{T} \qquad (5)$$

$A =$ pre-exponential factor, $E_a =$ activation energy, $R =$ ideal gas constant ($8.314\,\mathrm{J\,K^{-1}\,mol^{-1}}$)

Although the absence of an in-line detector and the resulting measurement inaccuracies cause notable deviations from the linear fit, the activation energy of the reaction can be estimated to $5.7 \pm 1.3\,\mathrm{kJ\,mol^{-1}}$, a value that is significantly lower than typical activation energies.[55] Assuming that the reaction does follow Arrhenius-like behavior, the reason for the seemingly low activation energy might be found in the formation of the acylpyridinium cation. Figure 9 illustrates the formation of the stabilized intermediate with a low activation barrier. Following this, the observed activation energy $E_{a,obs}$ consists of the enthalpy of the intermediate formation ΔH_1 and the activation energy of the rate-determining step $E_{a,2}$ [Equation (6)].

$$E_{a,obs} = \Delta H_1 + E_{a,2} \qquad (6)$$

DFT computations at the B3LYP/6-311+G(d,p)//B3LYP/6-31G(d) level of theory by Xu et al. result a similar energy diagram.[53] The energy levels found in this publication are quite different from our findings; however, these computations were done with a different substrate and in the gas phase. The polar silica surface, the high amount of catalyst during contact time, and the nonpolar solvent toluene (which favours ion pairing)[56]

in our reaction setup provide a unique environment that is likely to affect the stabilization of the intermediate.[57]

Conclusion

The DMAP organocatalyst was immobilized on silica particles and monoliths that were both optimized for continuous flow catalysis with respect to their pore space. The functionalization was performed in a two-step synthesis consisting of grafting of (3-azidopropyl)trimethoxysilane and copper catalyzed cyclo-addition of a DMAP alkynyl derivative. Silica particles were functionalized in batch and packed into a column, while monoliths were cladded in a PEEK tube and functionalized in circulating flow. Successful immobilization was confirmed by physisorption, infrared spectroscopy and elemental analysis. For both materials, three different loadings were synthesized, ranging from 0.2 to 0.9 mmol g^{-1}.

The high contact area between reactants and catalyst due to the large surface area of the mesoporous materials enables high yields up to complete conversion at short reaction times (<2 min). While packed-bed columns allow for easy analysis of properties prior to column packing and higher loadings are possible without loss of activity, monolithic reactors are superior in terms of conversion and pressure build-up. They outperform both packed-bed reactors and batch catalysis with turnover frequencies up to $9.3 \times 10^{-2}\,\mathrm{s^{-1}}$, which is competitive with TOFs for industrial applications of other organocatalysts.[52] For example, a commercially available 2,2,6,6-tetramethyl-piperidine-1-oxyl (TEMPO) derivative immobilized on silica reached a comparable TOF of $2.7 \times 10^{-2}\,\mathrm{s^{-1}}$ in a study of Michaud et al.[58] At high flow rates above $2\,\mathrm{mL\,min^{-1}}$, microkinetics become the determining factor for the reaction, i.e., diffusion-limitation can be excluded. This allows for meaningful analysis and comparison of activities. Kinetic studies with a monolithic
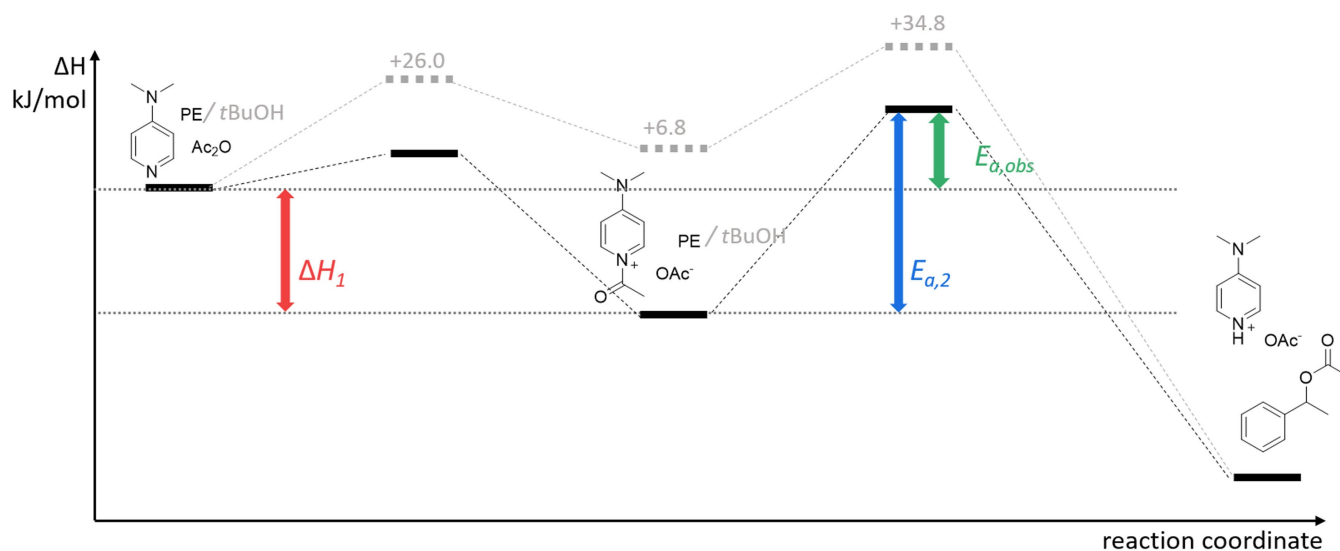

Figure 9. Reaction scheme for the explanation of the unexpectedly low observed activation energy $E_{A,obs}$. Note that the diagram is not to scale and does not depict real values of ΔH. Grey: DFT computations at the Becke3LYP/6-311+G(d,p)//Becke3LYP/6-31G(d) level of theory from Xu et al. (modified from [53]).

ChemCatChem

Research Article
doi.org/10.1002/cctc.202101845

**Chemistry
Europe**

European Chemical
Societies Publishing

reactor indicate a second order reaction, which is in accordance with the homogeneous reaction mechanism. The ideal transport properties of the monoliths possessing a high hydraulic permeability of 1.0×10^{-13} m^2 indicate that material restrictions are absent for the reactants, as also shown by Haas et al. who calculated a Thiele modulus of 10^{-4} for a similar catalyst material.[46] Therefore, one could argue that the reaction performed resembles a homogeneous rather than a heterogeneous reaction. The measured activation energy of 5.7 ± 1.3 kJ mol^{-1} is lower than expected from gas-phase DFT computations of Xu et al. although it is important to note that the observed activation energy might be a combination of the activation energy of the rate-determining step and the enthalpy of intermediate formation.

Our study shows that silica monoliths with bimodal pore structure have proven themselves suitable carrier materials for heterogeneous organocatalysis in continuous flow. The application of these materials to reactions with industrially relevant substrates might lead to improved productivity in continuous processing. Since the synthesis route is not exclusive for the DMAP derivative used in this work, various other organocatalysts can be immobilized in the same way and used in continuous flow. For instance, recently we showed that TEMPO-functionalized mesoporous silica particles can generally be used as oxidative catalyst system in flow.[59] The results of the present study indicate that enhanced catalytic performance might be achieveable for such demanding organocatalysts by using meso-macroporous monoliths.The complete synthesis of the reactor gives control over each step, so the material can be optimized for various catalysts and reactions by studying the effects of individual parameters like porosity and degree of functionalization to achieve a deeper understanding of continuous flow catalysis with porous silica materials.

Experimental Section

Materials

Silica particles were purchased from Merck (LiChrospher Si 100, 5 μm). Chemicals for synthesis were purchased from Merck/Sigma-Aldrich (sodium azide $\geq$ 99%, (3-chloropropyl)trimethoxysilane $\geq$ 97%, copper(I) iodide $\geq$ 97%, Bromotris(triphenylphosphine)copper(I) 98%, 4-(Methylamino)pyridine 98%, triethylamine > 99%, Urea 99.5%), Carl-Roth (N,N-diisopropylethylamine 99.5%, ethylenediaminetetraacetic acid disodium salt 99%), Alfa Aesar (propargyl acrylate 96% stabilized with 200 ppm BHT), Acros (tetramethoxysilane 99%, water-free solvents), and Fluka (polyethylene glycol 10.000). Solvents were purchased as HPLC grade (VWR) or distilled before use.

Essential Experimental Procedures/Data

Preparation of catalyst materials

DMAP click-derivative 0.251 g (2.32 mmol) N-methylaminopyridine and 1 mL (9.05 mmol) propargyl acrylate were stirred at 90 °C for 2 h. The excess of propargyl acrylate was removed through vacuum distillation, and the crude product was purified by column chromatography (DCM/MeOH 10:1, 1% NEt3). 0.358 g of a yellow liquid were obtained. ^{1}**H-NMR (400 MHz, CDCl$_3$):** δ (ppm) = 8.16 (d, 2H, pyridine-H), 6.45 (d, 2H, pyridine-H), 4.61 (d, 2H, R–CH$_2$–COOR), 3.65 (d, 2H, R-CH$_2$–CH$_2$–COOR), 2.93 (s, 3H, R–N–CH$_3$), 2.58 (t, 2H, RCH$_2$-C–CH$_3$), 2.42 (t, 1H, RCH$_2$-C–CH$_3$); **HRMS (ESI-TOF):** [M + H]$^+$ calculated for C$_{12}$H$_{14}$N$_2$O$_2$: m/z = 219.1128; found: m/z = 219.1128.

(3-azidopropyl)trimethoxysilane 1.76 g (27.1 mmol) dried sodium azide and 0.201 g (0.624 mmol) dried tetrabutylammonium iodide were dissolved in 15 mL dry acetonitrile. 1 mL (3-chloropropyl)trimethoxysilane were added and the mixture was stirred for five days at 90 °C. The solid residues were filtered off and the solvent was evaporated under reduced pressure. The crude product was dissolved in pentane and solid residues were removed by filtration. The purification steps were repeated until no solid residues precipitated out of the solution. 0.542 g (48%) of a colorless liquid were obtained. The purity of the product was determined to be 93% by NMR. ^{1}**H-NMR (400 MHz, CDCl$_3$):** δ (ppm) = 3.51 (s, 9H, RSi(OCH$_3$)$_3$, 3.20 (t, 2H, R-CH$_2$-N$_3$), 1.64 (p, 2H, R-CH$_2$-CH$_2$-N$_3$), 0.63 (t, 2H, Si-CH$_2$-R); **HRMS (ESI–TOF):** [M + Na]$^+$ calculated for C$_6$H$_{15}$N$_3$O$_3$Si: m/z = 228.0775; found: m/z = 228.0775.

Functionalization of silica particles with (3-azidopropyl)trimethoxysilane 100 mg silica (LiChrospher Si 100, 5 μm) were heated under vacuum for two hours. 4 mL dry toluene, 10 μL water and various amounts of (3-azidopropyl)trimethoxysilane (e. g. 8 μL, 16 μL, 36 μL) were added and the suspension was heated to 80 °C overnight in a shaking water bath. The material was washed with dichloromethane, methanol, and methanol/water (1:1) and dried at 80 °C. The azide loading of the functionalized materials was calculated with Equation (7):

$$X_{\text{azide}} = \frac{\%N}{N(N) \cdot M(N)} \tag{7}$$

X_{azide} = azide loading (mmol g^{-1}), $\%N$ = nitrogen content, $N(N)$ = number of nitrogen atoms in immobilized azide (= 3), $M(N)$ = molar mass of nitrogen

Functionalization of silica-azide particles with DMAP derivative Using copper iodide as catalyst: 50 mg of azide functionalized silica particles were suspended in 3 mL toluene. 40 μL of a 0.24 M (9.6 μmol) copper iodide solution in acetonitrile, 19 mg (0.085 mmol, 3.4 eq. in relation to azide on silica) DMAP derivative, and 101 μL (0.6 mmol) N,N-diisopropylethylamine were added. The solution was heated to 50 °C in a shaking water bath for three days. The material was washed successively with acetonitrile, methanol, Na$_2$EDTA (5 wt%), and water, in order to remove Cu salts, and finally dried at 80 °C. Using bromotris(triphenylphosphine)copper(I) as catalyst: 100 μL of a 0.06 mM CuBr(PPh$_3$)$_3$ solution was added instead of copper iodide.

The DMAP loading of the materials was calculated with Equations (8) and (9) on the basis of the nitrogen content:

$$\%N_{DMAP} = \frac{\%N_{EA} \cdot (100 - (\%N_{azide} + \%C_{azide} + \%H_{azide}))}{100 - (\%N_{EA} + \%C_{EA} + \%H_{EA})} \tag{8}$$

$$X_{DMAP} = \frac{\%N_{DMAP} - \%N_{azide}}{N_{add}(N) \cdot M(N)} \tag{9}$$

X_{DMAP} = DMAP loading (mmol g^{-1}), $N_{add}(N)$ = number of additional nitrogen atoms from DMAP functionalization (= 2)

Synthesis of silica monolith The synthesis of the monolith was adapted from Meinusch et al.[26] 1.200 g polyethylene glycol (10,000 g mol^{-1}) and 0.900 g urea were dissolved in 10 mL 0.01 M

ChemCatChem

Research Article
doi.org/10.1002/cctc.202101845

**Chemistry
Europe**
European Chemical
Societies Publishing

acetic acid and stirred for 35 min at 0 °C. 5.6 mL tetramethyl orthosilicate were added and the mixture was stirred at 0 °C for 20 min. The mixture was transferred in stainless steel tubes and tempered to 22.5 °C for 22 h. The monoliths were then transferred into a 0.01 M acetic acid solution containing 9 g urea per 100 mL for hydrothermal treatment (0.1 K min^{-1} to 95 °C, 95 °C for 15 h). After heating, the material was put into methanol and shaken gently on a laboratory shaker for five days, during which the methanol was replaced two times. For calcination, the monoliths were heated to 330 °C for 15 h. Monoliths with a length of 5 cm and a diameter of 0.3 cm were obtained. The cladding process was done as described in literature.[35]

Functionalization of silica monolith with azide The monolith (100 mg silica) was heated to 80 °C in a column oven and flushed with toluene for 15 min. A solution of toluene containing Az-PTMS (21 μL, 0.11 mmol for a resulting loading of 0.5 mmol g^{-1}) and triethylamine (15 μL, 0.11 mmol) was repeatedly pumped through the monolith for 18 h. After functionalization, the monolith was flushed with toluene for 15 min.

Functionalization of silica-azide monolith with DMAP derivative A solution of 2 mg (2.1 μmol) CuBr(PPh$_3$)$_3$, 70 μL (0.4 mmol) DiPEA, and 37 mg (0.17 mmol, 3.4 eq. in relation to azide on monolith) DMAP derivative in 10 mL toluene was passed through the azide monolith (0.5 mL h^{-1}). After functionalization, the monolith was flushed with 10 mL of an aqueous Na$_2$EDTA solution (5 wt%) and afterwards with 10 mL water (12 mL h^{-1}).

Characterization methods

The mesoporosity of the materials was examined with nitrogen physisorption. The measurements were done with a Quadrasorb evo (Quantachrome Instruments) at 77 K. Macroporosity was characterized with mercury intrusion porosimetry in a pressure range of 0–400 mPa (Pascal 140 and 440 porosimeter, Thermo Fisher Scientific).

For scanning electron microscopy, the materials were sputter-coated with platinum and measured with a Zeiss Merlin (acceleration voltage of 3 kV and a current of 90 pA). XPS analysis were done with a PHI5000 Versaprobe II Scanning ESCA Microprobe (Physical Electronics Inc) with a monochromatic Al K$_\alpha$ source (X-ray power 50 W). During the measurement, the sample surface was charge neutralized with slow argon ions and electrons and a pass energy of 23.5 eV was used for the detail spectra. The software CasaXPS was used for signal fitting using a Shirley background and a GL(30) line shape. The spectra were charge corrected with regards to the 284.8 eV peak of the C-1s signal. Diffuse reflectance infrared Fourier transform spectroscopy (DRIFT) was performed with a Bruker alpha. The spectra were recorded in a range of 400–4000 cm^{-1} with a resolution of 2 cm^{-1}. A CHN-analyzer Flash EA-1112 (Thermo Scientific) was used for elemental analysis. Nuclear magnetic resonance (NMR) spectra (^{1}H and ^{13}C measured with a Bruker Advance II 400 MHz instrument at 298 K) are reported as chemical shifts in ppm (multiplicity, coupling constants in Hz, assignment). A Bruker Daltonics MicroTOF II was used for exact mass analysis. Reaction yields of phenylethyl acetate were monitored via gas chromatography (HP 5890 Series II, capillary column DB-Wax 17, Agilent Technologies, FI detector).

Catalytic tests

For batch catalysis, 362 μL (3 mmol) 1-phenylethanol was dissolved in 10 mL toluene. Various amounts of catalyst material, 624 μL (4.5 mmol) triethylamine and 425 μL (4.5 mmol) acetic acid anhy-

dride were added and the mixture was stirred at room temperature.

Catalytic experiments with monoliths and packed-bed columns were performed with an HPLC pump (Hitachi L-600, Merck) and a column oven (Hitachi L-7300, Merck) with the same substrate concentrations as in batch catalysis. For long-term stability tests, acetic anhydride was added with a separate syringe pump.

Conflict of Interest

The authors declare no conflict of interest.

Data Availability Statement

The data that support the findings of this study are available on request from the corresponding author. The data are not publicly available due to privacy or ethical restrictions.

[1] W. Steglich, G. Höfle, *Angew. Chem. Int. Ed.* **1969**, *8*, 981.
[2] N. Bernhard, S. Wolfgang, *Angew. Chem. Int. Ed.* **1978**, *17*, 522–524; *Angew. Chem.* **1978**, *90*, 556–557.
[3] U. Ragnarsson, L. Grehn, *Acc. Chem. Res.* **1998**, *31*, 494–501.
[4] H. T. Chen, S. Huh, J. W. Wiench, M. Pruski, V. S. Y. Lin, *J. Am. Chem. Soc.* **2005**, *127*, 13305–13311.
[5] S. K. Chaudhary, O. Hernandez, *Tetrahedron Lett.* **1979**, *20*, 99–102.
[6] F. Nederberg, E. F. Connor, M. Möller, T. Glauser, J. L. Hedrick, *Angew. Chem. Int. Ed.* **2001**, *40*, 2712–2715; *Angew. Chem.* **2001**, *113*, 2784–2787.
[7] V. D'Elia, Y. Liu, H. Zipse, *Eur. J. Org. Chem.* **2011**, 1527–1533.
[8] E. Vedejs, X. Chen, *J. Am. Chem. Soc.* **1996**, *118*, 1809–1810.
[9] M. S. Xie, Y. F. Zhang, M. Shan, X. X. Wu, G. R. Qu, H. M. Guo, *Angew. Chem. Int. Ed.* **2019**, *58*, 2839–2843; *Angew. Chem.* **2019**, *131*, 2865–2869.
[10] Patent US20040180861 A1, **2004**.
[11] K. Shimoda, N. Kubota, *Molecules* **2011**, *16*, 6769–6777.
[12] D. Chen, B. Li, B. Li, X. Zhang, L. Wei, W. Zheng, *Green Process. Synth.* **2019**, *8*, 667–676.
[13] F. Cozzi, *Adv. Synth. Catal.* **2006**, *348*, 1367–1390.
[14] M. B. Gawande, P. S. Branco, R. S. Varma, *Chem. Soc. Rev.* **2013**, *42*, 3371–3393.
[15] Y. Qiao, A. D. Headley, *Catalysts* **2013**, *3*, 709–725.
[16] A. Sachse, A. Galarneau, F. Fajula, F. Di Renzo, P. Creux, B. Coq, *Microporous Mesoporous Mater.* **2011**, *140*, 58–68.
[17] P. H. R. de Oliveira, B. M. Bruno, R. A. C. Leão, L. S. M. Miranda, R. A. S. San Gil, R. O. M. A. de Souza, F. G. Finelli, *ChemCatChem* **2019**, *11*, 5553–5561.
[18] G. Mohammadi Ziarani, N. Lashgari, A. Badiei, *J. Mol. Catal. A* **2015**, *397*, 166–191.
[19] O. Bortolini, L. Caciolli, A. Cavazzini, V. Costa, R. Greco, A. Massi, L. Pasti, *Green Chem.* **2012**, *14*, 992.
[20] H. Ishitani, Y. Furiya, S. Kobayashi, *Bioorg. Med. Chem.* **2017**, *25*, 6229–6232.

[21] M. Colella, C. Carlucci, R. Luisi, *Supported Catalysts for Continuous Flow Synthesis*, Springer International Publishing, **2018**, vol. 376.

[22] K. Masuda, T. Ichitsuka, N. Koumura, K. Sato, S. Kobayashi, *Tetrahedron* **2018**, *74*, 1705–1730.

[23] E. Klemm, H. Döring, A. Geisselmann, S. Schirrmeister, *Chem. Eng. Technol.* **2007**, *30*, 1615–1621.

[24] K. Nakanishi, *J. Porous Mater.* **1997**, *4*, 67–112.

[25] K. Nakanishi, *Bull. Chem. Soc. Jpn.* **2006**, *79*, 673–691.

[26] R. Meinusch, R. Ellinghaus, K. Hormann, U. Tallarek, B. M. Smarsly, *Phys. Chem. Chem. Phys.* **2017**, *19*, 14821–14834.

[27] N. Tanaka, H. Nagayama, H. Kobayashi, T. Ikegami, K. Hosoya, N. Ishizuka, H. Minakuchi, K. Nakanishi, K. Cabrera, D. Lubda, *HRC J. High Resolut. Chromatogr.* **2000**, *23*, 111–116.

[28] K. Cabrera, *J. Sep. Sci.* **2004**, *27*, 843–852.

[29] S. Altmaier, K. Cabrera, *J. Sep. Sci.* **2008**, *31*, 2551–2559.

[30] G. Desmet, D. Cabooter, P. Gzil, H. Verelst, D. Mangelings, Y. Vander Heyden, D. Clicq, *J. Chromatogr. A* **2006**, *1130*, 158–166.

[31] A. Soliven, S. Pravadali-Cekic, D. Foley, L. Pereira, G. R. Dennis, K. Cabrera, H. Ritchie, T. Edge, R. A. Shalliker, *Microchem. J.* **2016**, *127*, 68–73.

[32] G. Guiochon, *J. Chromatogr. A* **2007**, *1168*, 101–168.

[33] K. Nakanishi, N. Tanaka, *Acc. Chem. Res.* **2007**, *40*, 863–873.

[34] K. Nakanishi, H. Minakuchi, N. Soga, N. Tanaka, *J. Sol-Gel Sci. Technol.* **1997**, *8*, 547–552.

[35] J. Chamieh, Y. Zimmermann, A. Boos, A. Hagège, *J. Chromatogr. A* **2010**, *1217*, 7172–7176.

[36] K. Turke, R. Meinusch, P. Cop, E. Prates Da Costa, R. D. Brand, A. Henss, P. R. Schreiner, B. M. Smarsly, *ACS Omega* **2021**, *6*, 425–437.

[37] H. K. Masao Tomoi, Yuzo Akada, *Makromol. Chem. Rapid Commun.* **1982**, *3*, 537–542.

[38] E. D. Alieva, N. I. Truhmanova, N. A. Platé, *Russ. Chem. Bull.* **1996**, *45*, 1226–1229.

[39] M. Benaglia, A. Puglisi, F. Cozzi, *Chem. Rev.* **2003**, *103*, 3401–3429.

[40] C. Ó. Dálaigh, S. A. Corr, Y. Gun'ko, S. J. Connon, *Angew. Chem. Int. Ed.* **2007**, *46*, 4329–4332; *Angew. Chem.* **2007**, *119*, 4407–4410.

[41] K. Motokura, M. Tomita, M. Tada, Y. Iwasawa, *Top. Catal.* **2009**, *52*, 579–585.

[42] N. A. Brunelli, W. Long, K. Venkatasubbaiah, C. W. Jones, *Top. Catal.* **2012**, *55*, 432–438.

[43] A. R. Bogdan, B. P. Mason, K. T. Sylvester, D. T. Mcquade, *Angew. Chem. Int. Ed.* **2007**, *46*, 1698–1701; *Angew. Chem.* **2007**, *119*, 1728–1731.

[44] Y. Okuno, S. Isomura, A. Sugamata, K. Tamahori, A. Fukuhara, M. Kashiwagi, Y. Kitagawa, E. Kasai, K. Takeda, *ChemSusChem* **2015**, *8*, 3587–3589.

[45] A. El Kadib, R. Chimenton, A. Sachse, F. Fajula, A. Galarneau, B. Coq, *Angew. Chem. Int. Ed.* **2009**, *48*, 4969–4972; *Angew. Chem.* **2009**, *121*, 5069–5072.

[46] C. P. Haas, T. Müllner, R. Kohns, D. Enke, U. Tallarek, *React. Chem. Eng.* **2017**, *2*, 498–511.

[47] R. Kohns, C. P. Haas, A. Höltzel, C. Splith, D. Enke, U. Tallarek, *React. Chem. Eng.* **2018**, *3*, 353–364.

[48] C. P. Haas, U. Tallarek, *ChemistryOpen* **2019**, *8*, 606–614.

[49] M. Thommes, K. Kaneko, A. V. Neimark, J. P. Olivier, F. Rodriguez-Reinoso, J. Rouquerol, K. S. W. Sing, *Pure Appl. Chem.* **2015**, *87*, 1051–1069.

[50] H. C. Kolb, M. G. Finn, K. B. Sharpless, *Angew. Chem. Int. Ed.* **2001**, *40*, 2004–2021; *Angew. Chem.* **2001**, *113*, 2056–2075.

[51] A. E. Fernandes, A. M. Jonas, O. Riant, *Tetrahedron* **2014**, *70*, 1709–1731.

[52] J. Hagen, *Industrial catalysis: A practical approach*, Wiley-VCH, Weinheim, 3rd edn. **2015**.

[53] S. Xu, I. Held, B. Kempf, H. Mayr, W. Steglich, H. Zipse, *Chem. Eur. J.* **2005**, *11*, 4751–4757.

[54] P. H. Y. Cheong, C. Y. Legault, J. M. Um, N. Çelebi-Ölçüm, K. N. Houk, *Chem. Rev.* **2011**, *111*, 5042–5137.

[55] G. Job, R. Rüffler, Vieweg + Teubner Verlag, Wiesbaden, 1st ed. 20. **2011**, p. 402.

[56] C. R. Martinez, B. L. Iverson, *Chem. Sci.* **2012**, *3*, 2191–2201.

[57] A. C. Spivey, S. Arseniyadis, *Angew. Chem. Int. Ed.* **2004**, *43*, 5436–5441; *Angew. Chem.* **2004**, *116*, 5552–5557.

[58] A. Michaud, V. Pandarus, L. Tremblay, R. Ciriminna, M. Pagliaro, F. Béland, *Top. Catal.* **2010**, *53*, 1110–1113.

[59] J. S. Schulze, J. Migenda, M. Becker, S. M. M. Schuler, R. C. Wende, P. R. Schreiner, B. M. Smarsly, *J. Mater. Chem. A* **2020**, *8*, 4107–4117.